colloids and interfaces

MDPI

Article

Discontinuous Shear Thickening of Suspensions of Magnetic Particles in Relation to the Polymer Coating on Their Surfaces

Georges Bossis [1,*], Olga Volkova [1] and Yan Grasselli [1,2]

[1] InPhyNi, Institut de Physique de Nice UMR 7010, CNRS, Université Côte d'Azur, 06200 Nice, France; olga.volkova@unice.fr
[2] SKEMA Business School, 60 Rue Dostoievski, BP085, 06902 Sophia Antipolis, France; yan.grasselli@skema.edu
* Correspondence: bossis@unice.fr; Tel.: +33-661108841

Abstract: The phenomenon of discontinuous shear thickening (DST) is observed in suspensions of solid particles with a very high-volume fraction. It is characterized by an abrupt decrease in the shear rate for critical stress during a ramp of stress. This behavior can be reproduced in numerical simulations by introducing a local friction between two particles above a given local force. We present experimental results showing this DST behavior obtained with suspensions of magnetic (iron) and nonmagnetic (calcium carbonate) particles and different amounts of a superplasticizer molecule used in the cement industry. For both types of particles, the same behavior was observed with first an increase in critical stress with the amount of plasticizer followed by a decrease at higher concentrations but with a larger viscosity before critical stress was reached. At a low concentration of plasticizer, the low critical stress is interpreted by the local sliding of plasticizer molecules on the surface of particles. At higher concentrations, when total coverage is achieved, the critical stress is higher since it has to remove the molecules out of the surface. At still higher concentrations, the increase in viscosity is explained by the formation of multilayers of molecules on the surface of the particles. This interpretation is supported by the measurement of the adsorption isotherm of the plasticizer on the surface of the particles.

Keywords: discontinuous shear thickening; adsorption isotherm; magnetorheology; carbonyl iron particles; calcium carbonate; superplasticizer

Citation: Bossis, G.; Volkova, O.; Grasselli, Y. Discontinuous Shear Thickening of Suspensions of Magnetic Particles in Relation to the Polymer Coating on Their Surfaces. *Colloids Interfaces* **2024**, *8*, 33. https://doi.org/10.3390/colloids8030033

Academic Editors: Cecile Lemaitre and Philippe Marchal

Received: 12 April 2024
Revised: 13 May 2024
Accepted: 15 May 2024
Published: 17 May 2024

1. Introduction

Mastering the rheology of suspensions of mineral particles is essential in many fields where these materials must flow in ducts before their final use. A few examples are cement or concrete in the construction of buildings or structures [1], the pastes made of a mixture of polymer and metallic particles for 3D printers [2], and the use of titanium dioxide or silica particles in numerous products like tooth paste [3], paints, paper coating [4], solar cream, etc. In most of these applications, we are looking for a paste which remains homogeneous and does not tend to aggregate at rest or during its flow, and for this, the physics of these suspensions must be understood [5]. To avoid the aggregation of the particles, and consequently their sedimentation or clogging, surfactant molecules are used, which have to provide a repulsive barrier on the surface of the particles. It can be achieved in different ways: using a polyelectrolyte molecule that provides an electrostatic repulsive force between ions of the same charge or with a coating of polymer either covalently bound to the surface or simply adsorbed through electrostatic interactions [6,7]. On the other hand, if these polymers have a good affinity with the solvent molecules, they provide a repulsive entropic force that prevents the polymers belonging to two different particles from interpenetrating each other. The resulting force between polymer brushes has been predicted by many authors [8–12] and depends mainly on the degree of polymerization and on the number of grafted chains per unit surface. If this force is not high enough to prevent

the particles from coming into contact, solid friction between particles occurs and creates a percolating network of particles. This network gives rise to discontinuous shear thickening (DST) as it was demonstrated by numerical simulations [13–15]. This phenomenon was observed a long time ago [16], and more recently, with different kinds of microparticles like corn starch [17], calcium carbonate (CC) [18,19], gypsum [20], poly~methyl methacrylate (PMMA) [21,22], ceramic [23], polystyrene [24,25], silica [25–28], carbonyl iron [29], etc. The DST transition can also appear with particles being sterically stabilized in non-polar solvents like PMMA in aliphatic hydrocarbon [22], in di-octyl phthalate [21], or stabilized by electrostatic layers in polar solvent like for quartz in water [26,27] or silica in water [28,30]. In a previous study on CC particles in water [19], a comparison of critical stress of the DST transition was made between three different brush polymers that electrostatically adsorb on the surface of the particles. An analytical expression for critical stress was obtained under the hypothesis that, above a given compression ratio, the polymer was expelled from the surface of the particles, providing the sudden percolation of a frictional network of particles. Such a hypothesis was also proposed in the study of the DST transition in a CC suspension in the presence of three other plasticizers [31].

In this study, we aim to find a quantitative interpretation of the correlation between the concentration of surfactant used and the evolution of critical stress when the DST transition occurs. After the Materials and Method Section, we shall present the rheological curves showing the DST transition at different concentrations of plasticizer for CC, carbonyl iron (CI), and a mixture of CC and CI particles. The Discussion Section is devoted to the interpretation of these experimental results with the help of the adsorption isotherm of the plasticizer molecule on CI and CC particles. Using a model of weak interpenetration of the polymer brushes [32] we consider the equality between the compression energy of the polymer and its adsorption energy as a criterion of expulsion of the polymer from the surface of the particles in the contact area; the relevance of this criterion is discussed.

2. Materials and Methods

The suspensions used are based on two kinds of particles, a CC powder produced by the company Omya, Oftringen, Switzerland, with the trademark BL200, and a CI powder (grade HQ produced by the company BASF, Ludwigshafen, Germany), which is currently used in the preparation of magnetorheological (MR) fluids [33,34]. The interest of MR fluids in the frame of the DST transition is that critical stress can be changed by the application of an external magnetic field [35,36]. The CC particles have an irregular shape, mainly rhomboidal (Figure 1a), whereas the CI particles are spherical (Figure 1b).

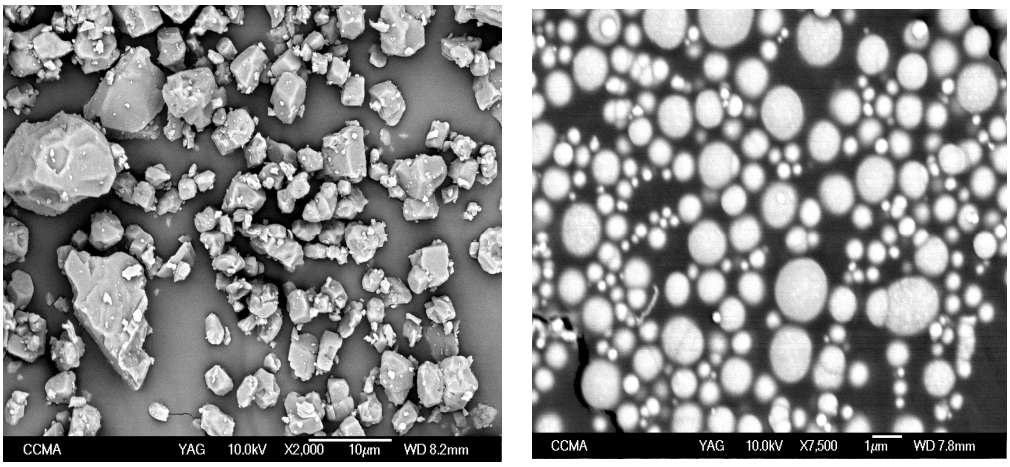

(**a**) (**b**)

Figure 1. SEM pictures of (**a**) calcium carbonate particles and (**b**) carbonyl iron particles.

The size distribution was obtained by analyzing, with the software ImageJ (ij154-win-java8), several images such as the ones presented in Figure 1a,b from scanning elec-

tron microscope (SEM) JEOL JSM 6700 (TEM, Tokyo, Japan). It is well represented by a lognormal distribution whose average radius and standard deviation are, respectively, a_{CC} = 1.75 μm and σ_{std_CC} = 0.809 μm and a_{CI} = 0.297 μm and σ_{std_CI} = 0.15 μm. A plot of the size distributions can be found in [35]. The densities of the particles were measured with a gas pycnometer (Accupyc II, Micromeritics, Norcross, USA), and ρ_{CC} = 2.72 g/cm^3 and ρ_{CI} = 7.7 g/cm^3. The superplasticizer is a polyelectrolyte whose commercial name is Optima 100 from Chryso company, Sermaises, France. It is made of a polyoxyethylene (PEO) chain of 44 units with a diphosphonate head (Figure 2). The counterions of the phosphonate group are sodium ions. The polymer is solvated in water at a concentration of 30 wt.%. The phosphonate head, negatively charged, binds with the positive ions, either calcium or iron, depending on the particles used. The suspending fluid is made of a mixture of ethylene glycol and de-ionized water (with resistivity of 18 MΩ·cm) in the ratio of 85–15%; it was chosen to minimize the evaporation of the solvent.

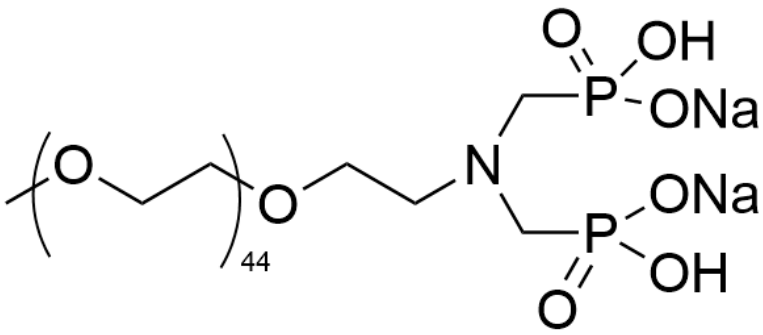

Figure 2. Chemical structure of the superplasticizer molecule, Optima 100.

The quantity of the polymer added to the suspending liquid is the weight of the dry polymer relative to the weight of the particles. After the addition of the mass of particles needed to obtain the required volume fraction, the suspension is stirred in a vortex during 5 min at 10 Hz, then placed in an ultrasound bath for 15 min (XTRA TT, Elmasonic, 400 W, 37 kHz), vortex stirred again for 5 min, and stored in a fridge for at least 12 h at 4 °C. Despite the presence of 15% of water in the suspending fluid, there was no oxidation sign like a rust color in the supernatant liquid after several days likely because the phosphates groups are known to have a good oxidation resistance. Just before its use in the rheometric cell, the suspension is still stirred in the vortex for 5 min and then briefly degassed under partial vacuum to remove remaining bubbles. The rheological results were obtained with a stress-imposed rheometer MCR 502 from Anton Paar with a parallel-plate geometry and a rotating disk of 40 mm diameter and a typical gap of 1 mm. To decrease wall slip, a sandpaper of 60 μm average roughness was stuck on both plates. The first step was a preshear with a ramp of stress between 0 and the maximum (typically 100 Pa) remaining below critical stress. The stress was maintained for 3 min and then stopped. After a rest time of 30 s, a linear ramp of stress was applied at a rate of 0.5 or 1 Pa/s. These rates were slow enough to obtain the equilibrium curves. For very concentrated suspensions, it is important that the constraints imposed by the compression of the suspension during the descent of the upper disk have time to relax. In the last step between 2 and 1 mm, the descent of the upper plate is regulated at a speed of 5 μm/s with a rotating speed of 0.1 rpm. The final position was then reached with a negligible axial force.

3. Results

In this section, we report experimental results obtained with three suspensions, one made of CC particles at a volume fraction of 68%, the second of CI particles at a volume fraction of 64%, and the third one being a mixture of the two previous types of particles with a total solid volume fraction of 70.5% with the percentage in mass of CI particles:

$m_{CI}/(m_{CI} + m_{CC})$ = 5%. In both situations, the weight ratio of Optima 100 is given as the ratio of the mass of dry polymer to the total mass of solid particles.

3.1. Suspension of Calcium Carbonate

The stress shear rate curve is given in Figure 3 for different weight percentages of the superplasticizer Optima 100; the total volume fraction being Φ_{CC} = 68%. It should be emphasized that, in the absence of Optima 100, it is not possible to obtain a flowing suspension at this volume fraction. In this figure, like in Figures 4 and 5, it can be noted that the shear rate is unstable above the critical shear stress. This is a common feature found in DST transitions where the differential viscosity becomes negative and produces an instability on the shear rate at imposed shear stress [25–27,36].

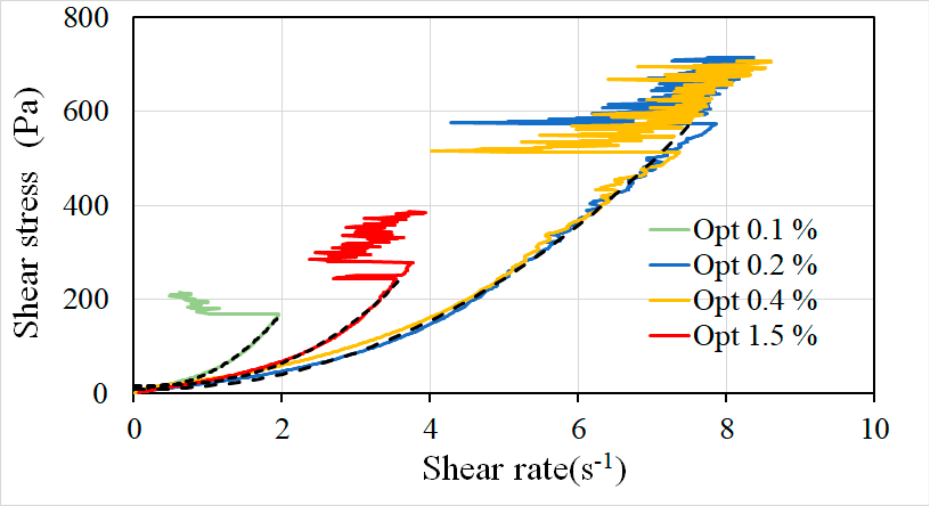

Figure 3. Shear stress versus shear rate for a suspension of calcium carbonate at a volume fraction Φ = 68% and different weight ratios of Optima 100. The dashed lines are fits based on the Herschel–Buckley law.

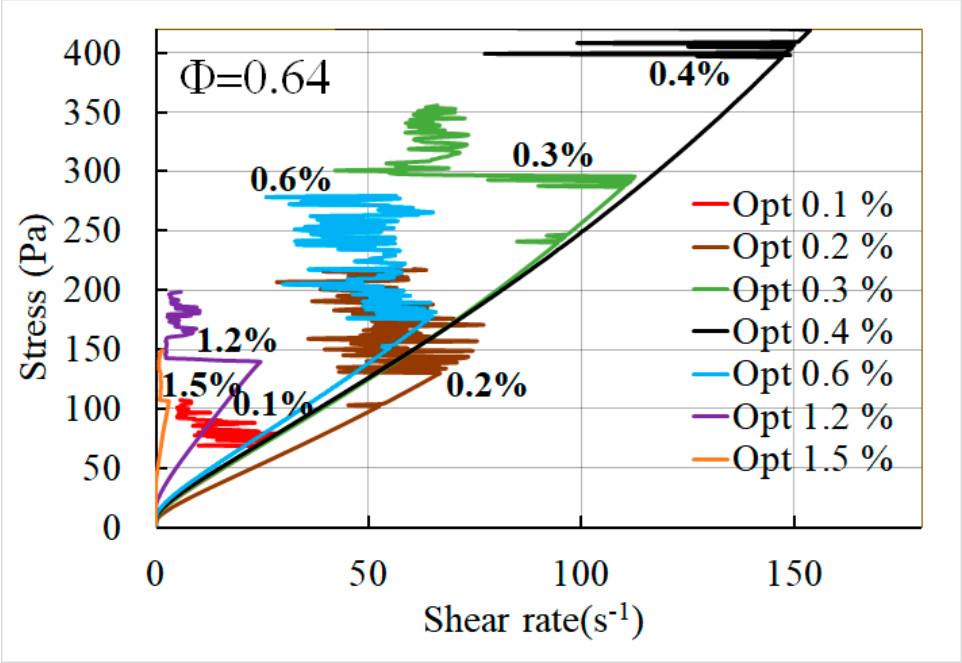

Figure 4. Shear stress versus shear rate in a suspension of carbonyl iron at a volume fraction of 64% and different weight ratios of Optima 100.

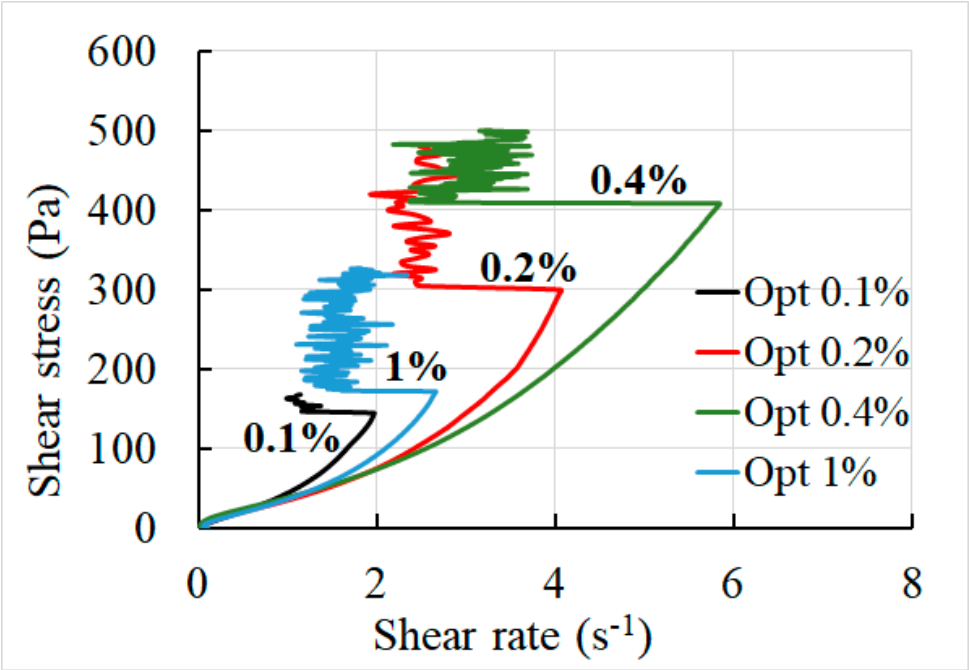

Figure 5. Shear stress versus shear rate in a suspension made of 95 wt.% of CC particles and 5 wt.% of CI particles for a total volume fraction Φ_{tot} = 70.5%. The weight percentage of Optima is still relative to the total weight of solid.

The initial viscosity is the highest at 0.1% (η = 41 Pa·s) and the lowest at 0.2% (η = 22 Pa·s), but the most impressive change is critical stress that increases from 169 Pa at 0.1% to 573 Pa at 0.2%. There is no significant change up to 0.4%, but when the percentage of Optima increases further, a plateau is not reached as could be expected. Instead, we observe a strong decrease in critical stress down to 271 Pa. The fit of the curves below the transition point was based on the Herchel–Buckley (HB) law: $\sigma = \tau_y + K.\dot{\gamma}^n$ is represented with a black dashed line for 0.1%, 0.2%, and 1.5%. The exponent, n, of the power law is minimum and equal to 1.98 for 0.2% and 0.4% but larger for 0.1% (n = 2.7) and maximum for 1.5% (n = 3.1). It then appears that a too large quantity of polymer increases the shear thickening behavior before the DST transition. Nevertheless, at the same time, it facilitates this transition since critical stress is much lower than at 0.2%. Let see now what happens with the CI suspension when we change the quantities of Optima 100.

3.2. Suspension of Carbonyl Iron

In Figure 4, the results are plotted for a total volume fraction, Φ = 0.64, and seven different percentages of Optima 100. The change in behavior is still more important than that for the suspension of CC particles, but the same trend is maintained with low critical stress at 0.1%, the maximum at 0.4%, and a continuous decrease above 0.4% together with a very large increase in viscosity. Also, contrary to the CC suspension, the rheology is not far from Newtonian, and, at the highest percentage of Optima 100, a slight shear thinning occurs before the transition instead of the expected shear thickening. This observation was already made when looking at the change in the DST transition for the same suspension, but in the presence of a magnetic field of different magnitudes instead of a change in the plasticizer concentration (Figure 13b in [35]). It means that, contrary to the model currently used to reproduce the DST transition [37], this transition is not the result of a continuous increase in the fraction of frictional contacts until percolation across the measuring cell appears, but is rather due to a sudden expulsion of the coating layer that was preventing the particles from coming into contact. We shall come back to this point in the next section.

In Table 1, the values are reported for critical stress, σ_c, viscosity $\eta_c = \frac{\sigma_c}{\dot{\gamma}_c}$, where $\dot{\gamma}_c$ is the critical shear rate, and exponent n of the HB fit. The fitted curves are not represented

because they cannot be distinguished from the original ones. Looking at the values of the last line, we see that, both at low (0.1%) and high concentrations (1.2% and 1.5%), there is some shear thinning (n < 1), and it is maximum around n = 1.2, corresponding to the domain of high critical stress. Compared to calcium carbonate in which the increase in viscosity is twice at the highest value of Optima 100 (1.5%), here, there is more than one order of magnitude between 0.2% and 1.5%.

Table 1. Critical stress, viscosity at the transition point, and exponent of the HB law for different weight fractions of Optima in a suspension of CI particles at $\Phi = 0.64$.

wt%	**0.1%**	**0.2%**	**0.3%**	**0.4%**	**0.6%**	**1.2%**	**1.5%**
σ_c	76.20	130.60	292.00	396.20	175.10	140.07	106.05
η_c	2.80	2.00	2.61	2.69	2.73	5.70	33.56
n	0.84	1.09	1.22	1.25	1.05	0.87	0.74

This increase in viscosity above roughly 1 wt.% of Optima 100 deserves an explanation that is given in the next section.

3.3. Mixture of Calcium Carbonate and Carbonyl Iron

In a previous study [35], we have shown that a small fraction (5% in volume) of CI particles among CC particles was enough to monitor the viscosity and the DST transition of the mixture with a low magnetic field; the interest was in reducing the sedimentation of the iron particles, which remains a major problem in the use of MR fluids. For this composition, it is interesting to see how the rheological behavior changes as a function of the proportion of Optima 100. The results are presented in Figure 5.

The main feature concerning the presence of an optimum percentage around 0.4% is still present, and the global behavior with a strong shear thickening is similar to the one observed with the CC particles alone (Figure 3). This was expected since the percentage of CC particles is 95%, so the 5% of iron particles should not critically impact the global behavior. In the following discussion, we try to answer the following questions: (1) is it possible to explain qualitatively the behavior of critical stress with the concentration of the superplasticizer? and (2) is it possible to obtain a quantitative prediction of critical stress from the knowledge of the interaction forces between particles? To answer these questions, we need to, at least, correlate the concentration of plasticizer to the density of adsorption of these molecules on the surface of the particles.

3.4. Adsorption Isotherm of CC and CI Particles for Determination of Adsorption Energy

The adsorption isotherm was measured by the method of Total Organic Carbon (TOC-VCSH Shimadzu), where a known mass of polymer relative to the mass of particles is added to the suspending liquid and placed on a rotating stirrer for 12 h. After centrifugation, the supernatant liquid is calcined at 680 °C, and the residual carbon is determined by infrared absorption of gaseous CO_2. After calibration with known quantities of Optima 100, the quantity remaining in the supernatant is measured and therefore what is adsorbed on the surface of the particles. In these experiments, we took 5.1 g of calcium carbonate and 30 g of carbonyl iron.

The Langmuir model is based on the equality between the chemical potential of the molecule in the liquid phase and on the surface of the particle [38]. It gives the following prediction for the adsorbed mass, m_{ads}, of polymer versus its initial mass concentration $C_{init} = m_{init}/V$ (g/cm^3) in the liquid phase of volume V:

$$m_{ads} = m_{sat}\frac{b.C_{init}}{1 + b.C_{init}} \; with \; b = \frac{10^3}{m_{opt}}.e^{\frac{-\varepsilon}{kT}}\left(\frac{h^2}{2\pi m_{opt}kT}\right)^{\frac{3}{2}} \quad (1)$$

where m_{sat} is the mass of polymer at the plateau of adsorption, h is the Planck constant, m_{opt} is the mass of the Optima 100 molecule (m_{opt} (kg) = $2.2/N_{av}$ with N_{av} the Avogadro number), and ε is the adsorption energy on the surface of the particle. The prefactor $10^3/m_{opt}$ is due to the change in unity from number per m^3 to g/cm^3. In Figure 6, we report the experimental adsorption and the fit of the Langmuir equation for the two types of particles. First, it can be noted that the adsorption is stronger for the CC particles since, to obtain a coverage of 60% surface, the initial concentration is approximately four times less for the CC than for the CI particles. The fit with the Langmuir model gives m_{sat} = 5.22 mg and b = 4360 for CC particles and m_{sat} = 108 mg and b = 878 for CI particles, respectively. From Equation (1), we find that $\varepsilon/kT = -28.1$ for CC particles compared to $\varepsilon/kT = -26.5$ for CI ones, showing that the binding energy with the surface is less important for the CI particles. The initial adsorption energy at a low concentration of polymer on the surface is well represented by the Langmuir model, but when the coverage increases, it is no longer the case because the excluded volume interactions between the molecules on the surface are not taken into account, so we need to be cautious with the absolute value of the total adsorbed mass, m_{sat}, given by this model, but it can be used to interpret qualitatively the effect of the concentration of this molecule on the rheology.

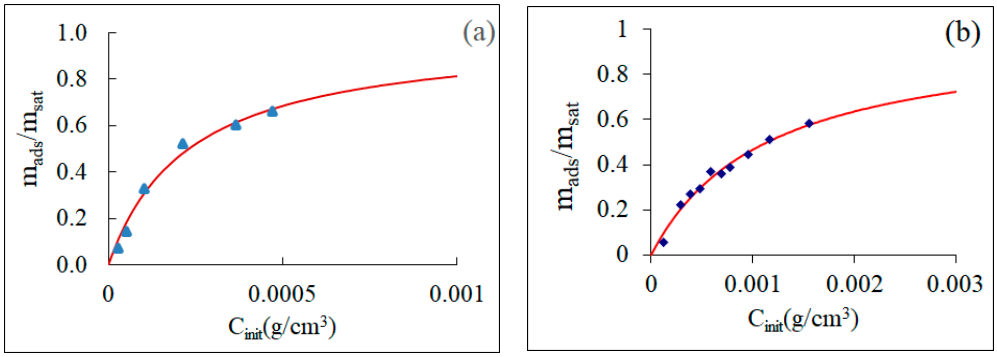

Figure 6. Adsorption isotherms of Optima 100 on particles of (**a**) calcium carbonate$_3$ and (**b**) carbonyl iron. The red solid line represents a fit by the Langmuir model.

3.5. Extrapolation of Adsorption Isotherm under the Conditions of Rheology Experiments

It is worth noting that the important changes in critical stress reported in Figures 3–5 are obtained at plasticizer concentrations that are much higher than those used in the isotherm measurements. For instance, the weight concentration of 0.1 wt.% (ratio of the mass of plasticizer to the mass of particles), used for the suspension of CC at Φ = 0.68, corresponds to 0.0053 g/cm^3, which is well beyond the concentrations used for the isotherm presented in Figure 6. The points corresponding to the volume concentrations used in the rheological experiments are shown in Figure 7a,b, and are versus the weight ratio instead of C_{init} in abscissa. The Langmuir equation remains the same but with a new coefficient $b' = m_{CC}\, b/(10^3 \cdot V_{liq})$, with V_{liq} and m_{CC} being the volume of liquid and the mass of particles (either CC or CI) used in the rheological experiments, respectively. m_{opt} is the mass of one Optima 100 molecule.

We observe that the concentrations of plasticizer used in the rheology experiments correspond to a coverage between 92% and more than 99% for the two last points at wt = 0.012 and wt = 0.015. Then, with the mass ratio in abscissa, quite similar predictions for the coverage fraction of surfaces are obtained, since for wt = 0.002, we have 0.98 for CC particles and 0.96 for CI particles.

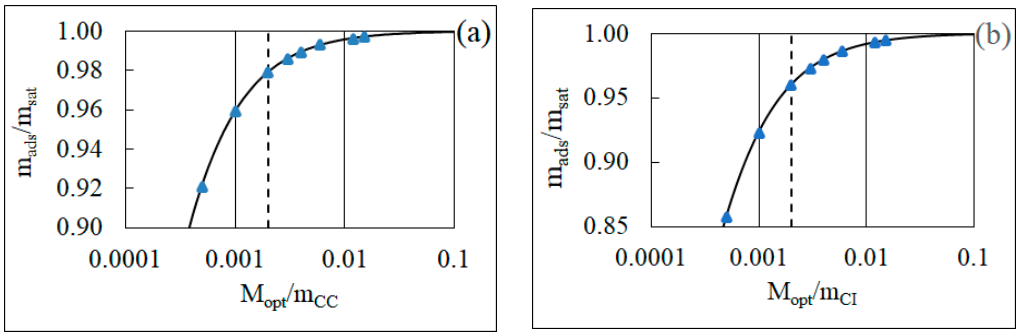

Figure 7. Coverage fraction of plasticizer molecules deduced from the Langmuir isotherms for the weight fractions used in the rheological experiments: (**a**) for CC particles and (**b**) for iron particles. The dashed vertical lines correspond to M_{opt}/m_{CC} = 0.002 = 0.2 wt.%.

4. Discussion

First, the information provided by the adsorption isotherms of Figure 7a,b is used to help understand the change in the rheology of these concentrated suspensions when the concentration of Optima 100 is varied. Then, an attempt is be made to predict critical stress from the local forces between two particles with the hypothesis that the DST transition occurs when the energy of compression of the polymer is equal to its adsorption energy.

4.1. Interpretation of the Increase in Critical Stress Up to wt = 0.4%

The first point at wt = M_{opt}/m_{CC} = 0.0005 in Figure 7a,b was not used in the rheology experiments because it was not possible to obtain a homogeneous liquid phase in the rheometer gap for this concentration. It appears that a large increase in critical stress between wt = 0.001 and wt = 0.004 is related to reaching a full surface coverage (>98%) of the particles. On the other hand, one might wonder why a small variation in coverage from approximately 96% to 98% can produce such a big change in critical stress (Figures 3–5). A possible explanation is that, since some free space remains on the surface, when two particles are pushed against each other by the shear force, the adsorbed molecules can slide on the surface and move away from the contact zone allowing a frictional contact between the particles. It is only when total coverage is reached that this sliding motion becomes forbidden and that the force necessary to expel the plasticizer molecules from the surface becomes much more important. Nevertheless, it does not explain why, when the concentration of plasticizer molecules is still increased, critical stress decreases, and at the same time, viscosity increases.

4.2. Interpretation of the Decrease in Critical Stress for wt > 0.4%

If After the completion of the first layer, the concentration of plasticizer molecules in the liquid phase is increased, the polymer continues to adsorb, either forming a bilayer with the PEO chains in contact and the phosphonate head remaining in contact with the liquid phase or as spherical micelles or both at the same time. During a collision between two particles, a bridge made of a concentrated solution of polymer forms in the gaps between the particles with a local viscosity, η_m, that is much higher than the one of the solvent, η_{m0}. The effect of the thickness of the polymer layer on viscosity can be related to the effective volume fraction. If we call $R + \delta R$ the radius of the particle plus its shell of polymer, the effective volume fraction increases such that we obtain the following:

$$\Phi_{eff} = \frac{V_1}{V_1 + \frac{(1-\Phi)}{\Phi} V_0} V_0 = \int_0^\infty P_{log}(R) R^3 dR;\ V_1 = \int_0^\infty P_{log}(R+R)(R+R)^3 dR$$

where P_{log} is the lognormal distribution, whose parameters are given in Section 2, V_0 is the volume of the bare particles, and V_1 is the volume that includes the shell of the polymer. To calculate Φ_{eff}, the thickness of the polymer layer is needed. We see below that this thickness

can be close to 15 nm. For CI particles, the maximum volume fraction characterized by the divergence of viscosity of frictionless particles is $\Phi_m = 0.678$ [35]. Starting from $\Phi = 0.64$ and a bilayer of polymer of thickness $\delta R = 30$ nm, $\Phi_{eff} = 0.672$, which is very close to the maximum volume fraction. As most of the dissipation occurs in the gaps between the particles, it means that the suspending fluid has an effective viscosity close to the one of a concentrated polymer, which is very high. For instance, Optima 100 at a mass concentration of 83% in water has a viscosity of 3.95 Pa·s compared to a viscosity of 0.013 Pa·s at a mass concentration of 30%. This ratio of more than two orders of magnitude can easily explain the increase in viscosity by a factor of 35 between wt.% = 0.2% and wt.% = 1.5% (Figure 4). At the same time, it explains the decrease in critical stress because it is the local stress, $\sigma_m = \eta_m \dot{\gamma}_{loc}$, and not the average one, which acts inside the gap between surfaces and expels the polymer from the surface of the particles. Also, it is likely that the presence of another layer of polymer or of micelles at the surface of the first layer contributes to the decrease in its adsorption energy and thus to lower critical stress. For the CC suspension, the increase in viscosity and the decrease in critical stress at the highest concentration of polymer are not very important (Figure 3); the viscosity at the transition point increases from 77.7 Pa·s to 84 Pa·s between wt.% = 0.2% and wt.% = 1.5%, and critical stress is divided by two. This is qualitatively understandable since the average diameter being six times larger than the one of CI particles, the same increase in thickness of the polymer layer has a lesser effect on the change in the effective volume fraction. For instance, with a thickness of 30 nm, $\Phi = 0.68$ transitions to $\Phi_{eff} = 0.687$, which is still far from the maximum volume fraction, i.e., $\Phi_{max} = 0.72$.

4.3. Attempt to Predict Critical Stress

A more quantitative insight into critical stress can be obtained from the expression of the forces between particles. In addition to the well-known van der Waals force, the repulsive force between two polymer layers depends mainly on their interpenetration depth and on their packing density. Different models have been proposed [10,12,39–41] mainly based on the scaling theory derived from De Gennes's study [39]. Molecular dynamic simulation allows to check these models, and R. Desai et al. [32] found a good agreement with simulations in the regime of small interpenetration between the two polymer brushes. As this regime seems to be adapted for a layer of densely packed polymer, we use it to describe the forces between two particles. The repulsive interaction energy, U, per unit area between two plates separated by a distance h is given by the following [41]:

$$\frac{U(h, d_0, D_s)}{kT} = C_\nu \frac{1}{b_0^2}\left(2 - \frac{h}{d_0}\right)^{\frac{5\nu}{5\nu-1}} \text{ with } C_\nu = P^{\frac{1+5\nu}{5\nu-1}}\left(\frac{b_0^2}{D_s^2}\right)^{\frac{7+15\nu}{3(5\nu-1)}} \quad (2)$$

In this expression, d_0 is the equilibrium thickness of the polymer layer, and D_s is the average distance between two polymers adsorbed on the surface. The exponent ν depends on the quality of the solvent, i.e., $\nu = 1/2$ for a θ solvent and $\nu = 3/5$ in a good solvent, where the contribution of the excluded volume between monomers to the entropy is considered [42]. $P = 44$ is the number of monomers. The Kuhn length of the PEO chain is $b_0 = 0.52$ nm [43,44], deduced from the end to end distance, i.e., $< r^2 >= 2\lambda P l_m = P b_0^2$, where $l_m = 0.36$ nm and is the projected length of a monomer, and $\lambda = 0.37$ nm and is the persistence length [44]. The repulsive force between two spherical particles of radius R is then given by the Derjaguin approximation [45]:

$$F_{rep} = \pi R\, U(h, d_0, D_s) \quad (3)$$

The repulsive energy between two spherical particles is given by the integral of Equation (3) between $h = 2d_0$, where $F_{rep} = 0$, and h:

$$W_{rep} = \pi\, R\, kT \frac{C_\nu}{b_0^2} \frac{5\nu - 1}{10\nu - 1} d_0 \left(2 - \frac{h}{d_0}\right)^{\frac{10\nu-1}{5\nu-1}} \quad (4)$$

The equilibrium thickness, d_0, of the adsorbed layer can be obtained in the Flory approach by a minimization of the free energy relative to d_0 in a cylindrical volume $V \sim d_0 D_s^2$ [42]. The contribution of the excluded volume $v \sim b_0^3$ and of the mixing energy parameter, χ, between the polymer and the solvent is taken into account and gives the following result [12]:

$$d_0 \sim P \left(w b_0^2 / D_s^2\right)^{\frac{1}{3}} \text{ with } w = b_0^3(1 - 2\chi) \quad (5)$$

This expression reduces to the one given in [41,46] with $\nu = 3/5$ and $\chi = 0$ (theta solvent). We consider $\chi = 0.36$ for the Flory parameter [47] The two other forces acting between a pair of particles come from the shear stress and from the van der Waals interaction:

$$F_{sh} = \sigma\, (2R)^2 \text{ and } F_{VDW} = -A_h \mathrm{R} / \left(12h^2\right) \quad (6)$$

A_h is the Hamaker constant; $A_h = 2.23 \times 10^{-20}$ for $CaCO_3$ [48] and $A_h = 10^{-19}$ for iron [49]. The abrupt transition observed in Figures 3–5 suggests that it is linked to the expulsion of the polymer that happens when the energy stored during the compression of the polymer layers exceeds the adsorption energy. We can then obtain the critical distance, h_c, by equating W_{rep}/kT to ε/kT. Then, critical stress, σ_c, is obtained from the balance of forces:

$$\sigma_c \pi R^2 + F_{rep}(h_c) + F_{VDW}(h_c) = 0 \quad (7)$$

The only unknown here is D_s, i.e., the average distance between adsorbed polymers. The number of adsorbed molecules, i.e., $N_{ads} = m_{ads}/m_{opt}$, for a given initial concentration of polymer is known from the Langmuir model, and the surface of the particles is obtained from the measurement of the specific surfaces by the BET method, which is $S_{spCC} = 0.54\ m^2/g$ for CC particles and $S_{spCI} = 0.45\ m^2/g$ for CI particles. The minimum distance, D_{min}, between adsorbed polymers at the saturation plateau is given by the values of the adsorption isotherm since the number of molecules in one layer on the surface is $N_s = m_{sat}/m_{opt}$. As the total surface of CC particles is $m_{CC} S_{spCC}$, we have the following:

$$D_{min} = \sqrt{\left(m_{CC} S_{spCC}\right)/N_s} \text{ and } \frac{D_s(C_{init})}{D_{min}} = \sqrt{\frac{m_{sat}}{m_{ads}(C_{init})}} = \sqrt{\frac{(1 + bC_{init})}{bC_{init}}} \quad (8)$$

where $m_{cc} = 5.1$ g and $m_{sat} = 5.22$ mg refer to the values of the adsorption isotherm of Optima 100 on CC particles. The second equation, derived from Equation (1), gives the change in average distance with the initial concentration, C_{init}, if the molecules are distributed equidistantly on the surface, but a phase separation can occur beyond a given coverage fraction. The application of Equation (8) gives $D_{min} = 1.39$ nm on the surface of CC particles. The measurement of the adsorption isotherm of Optima 100 on the surface of CI particles was made with $m_{CI} = 30$ g and $m_{sat} = 108$ mg, giving $D_{min} = 0.68$ nm. It is interesting to compare these distances to the gyration radius of Optima. The gyration radius of a PEO chain was deduced from static and dynamic light scattering for different molecular weights and was found to be [50] $R_G = 0.0215 M_w^{0.583} = 1.91$ nm for Mw = 2200 g/mol. An other recent study [51] based both on simulations and double electron–electron resonance gives $R_G = 0.019\ M_w^{0.588} = 1.74$ nm. By comparison with D_{min}, it is obvious that the adsorbed polymer is strongly compressed in the dimension parallel to the surface, but in practice, the polymers interpenetrate to gain configurational entropy [46]. The fact that the polymer

density is higher on the iron surface comes from the higher density of the iron atoms than that of calcium atoms on the surface of CC particles. From the knowledge of D_s or D_{min} at the adsorption plateau, the height d_0 of the adsorbed layer can be obtained (Equation (5)). Taking $\nu = 3/5$ for our case, where the PEO is in a good solvent, thickness $d_0 = 7.5$ nm for the CC particles and $d_0 = 12.4$ nm for CI particles. This last value is not far from the length of the completely stretched polymer: $L = 44 \times 0.36 = 15.8$ nm. Using $D_{min} = 1.39$ nm for the average distance between the polymers on the CC particles and $W_{rep}/kT = \varepsilon/kT = -28.1$ for its adsorption energy, the solution of Equations (4)–(7) gives critical stress: $\sigma_c = 142$ Pa. For the CI particles, with $D_{min} = 0.68$ nm and $W_{rep}/kT = \varepsilon/kT = -26.5$, critical stress $\sigma_c = 10{,}300$ Pa. Experimentally, the maximum critical stress obtained for 0.4% wt is between 400 and 600 Pa for the three systems that we studied (Figures 3–5). Thus, for CC particles, this model underpredicts critical stress by a factor of three, and for CI particles, it overpredicts critical stress by more than one order of magnitude. The large difference between the predictions for CC particles and CI particles is mainly due to their size difference: considering the size of the CI particles as the size of CC particles, the model predicts $\sigma_c = 576$ Pa instead of 10,300 Pa. This high sensitivity to the size of the particles is because the hydrodynamic force on a pair of particles scales like σR^2 (Equation (7)), whereas the repulsive force and the van der Waals force scales only as R. It is worth noting that this simple model aiming to relate critical stress to the force acting on a pair of particles is independent of the volume fraction of the suspension. This is certainly not the case since the jamming transition is related to the percolation of a network of particles in frictional contact, which implies a volume fraction larger than 0.55–0.56: the loose random packing fraction for monosized hard spheres [15]. In these highly concentrated suspensions, transient aggregates are formed within which stress is transmitted as in a solid, so the basic scale is no longer the particle but an aggregate of particles, and the hydrodynamic force between aggregates of particles is now proportional to the square of the diameter of these aggregates. This interpretation recalls the one from Wyart-Cates [37] who introduced a critical volume fraction for the jamming transition that depends on a phenomenological function, $f(\sigma)$, of the applied stress representing the fraction of particles in frictional contacts. The fact that one faces a multiscale interaction, not mentioning the initial polydispersity, makes a good prediction of critical stress difficult, but new experiments, particularly with different sizes of particles obtained by sieving the same initial powder, should help in understanding why critical stress seems experimentally quite independent of the size of the particles, contrary to the prediction of a theoretical approach based on pair interactions between particles.

5. Conclusions

Critical stress characterizing the discontinuous shear thickening transition was measured for suspensions composed of different particles (calcium carbonate, carbonyl iron, or a mixture of the two), but with the same molecule of superplasticizer. For the three types of suspensions, the same behavior was observed during the increase in the concentration of the plasticizer, namely, an increase in critical stress, followed by a plateau, and then a decrease accompanied by a growth in viscosity or the shear thickening effect before the transition. From the fit of the adsorption isotherm by the Langmuir model, we have found that the adsorption energy of the plasticizer polymer on carbonyl iron particles was slightly smaller (26.5 kT against 28.1 kT) than that on calcium carbonate particles. By reporting the concentrations of plasticizer used in the rheological measurements on the Langmuir curve, it appears that the surface of the particles was close to fully covered by a monolayer of polymer. The important increase in critical stress between 0.1% wt and 0.4% wt was associated with the completion of this monolayer, whereas an excess of plasticizer likely acts towards destabilizing this monolayer by forming a polymer melt in the gap between the particles that increases the local viscosity and favors the removal of the polymer from this zone of contact. Finally, with the hypothesis that the polymer is removed out of the surface of the particles in the contact zone, when the energy of compression of the polymer becomes larger than its adsorption energy, we obtain, without any adjustable parameter,

the right order of magnitude of critical stress for CC particles but an order of magnitude higher for the CI particles. This last discrepancy is associated with the much smaller size (by a factor of five) of the CI particles since the shear force on a pair of particles decreases as R^2. The fact that the experimental critical stress is quite insensitive to the size of the particles could be due to the aggregation process that transposes the magnitude of the shear forces between two particles at the scale of these aggregates.

Author Contributions: Conceptualization and writing: G.B.; investigation: O.V.; software: Y.G. All authors have read and agreed to the published version of the manuscript.

Funding: The authors want to thank the CENTRE NATIONAL D'ETUDES SPATIALES (CNES, the French Space Agency) for supporting this research (contract N°: 4500076631).

Data Availability Statement: The excel files of the figures are available upon request from the corresponding author.

Acknowledgments: We are grateful to R. Morini and Y. Ismaylov for measuring the adsorption isotherm for CC and CI particles, respectively.

Conflicts of Interest: The authors declare no conflicts of interest. The funders had no role in the design of the study; in the collection, analyses, or interpretation of data; in the writing of the manuscript; or in the decision to publish the results.

References

1. Kabashi, V.; Liberto, T.; Robisson, A. Shear-Induced Particle Migration in a Cement Slurry under Oscillatory Pipe Flow. *J. Non-Newton. Fluid Mech.* **2023**, *319*, 105071. [CrossRef]
2. Roshchupkin, S.; Kolesov, A.; Tarakhovskiy, A.; Tishchenko, I. A Brief Review of Main Ideas of Metal Fused Filament Fabrication. *Mater. Today Proc.* **2021**, *38*, 2063–2067. [CrossRef]
3. Sarcev, B.P.; Zlatanovic, D.L.; Hadnadjev, M.; Pilic, B.; Sarcev, I.; Markovic, D.; Balos, S. Mechanical and Rheological Properties of Flowable Resin Composites Modified with Low Addition of Hydrophilic and Hydrophobic TiO2 Nanoparticles. *MATERIALE PLASTICE* **2021**, *58*, 80–90. [CrossRef]
4. Chen, H.; Wang, B.; Li, J.; Ying, G.; Chen, K. High-Strength and Super-Hydrophobic Multilayered Paper Based on Nano-Silica Coating and Micro-Fibrillated Cellulose. *Carbohydr. Polym.* **2022**, *288*, 119371. [CrossRef]
5. Ness, C.; Seto, R.; Mari, R. The Physics of Dense Suspensions. *Annu. Rev. Condens. Matter Phys.* **2022**, *13*, 97–117. [CrossRef]
6. Borkovec, M.; Szilagyi, I.; Popa, I.; Finessi, M.; Sinha, P.; Maroni, P.; Papastavrou, G. Investigating Forces between Charged Particles in the Presence of Oppositely Charged Polyelectrolytes with the Multi-Particle Colloidal Probe Technique. *Adv. Colloid Interface Sci.* **2012**, *179*, 85–98. [CrossRef] [PubMed]
7. Azzaroni, O. Polymer Brushes Here, There, and Everywhere: Recent Advances in Their Practical Applications and Emerging Opportunities in Multiple Research Fields. *J. Polym. Sci. A Polym. Chem.* **2012**, *50*, 3225–3258. [CrossRef]
8. Alexander, S. Adsorption of Chain Molecules with a Polar Head a Scaling Description. *Journal De Physique* **1977**, *38*, 983–987. [CrossRef]
9. De Gennes, P.G. Conformations of Polymers Attached to an Interface. *Macromolecules* **1980**, *13*, 1069–1075. [CrossRef]
10. Milner, S.T.; Witten, T.A.; Cates, M.E. Theory of the Grafted Polymer Brush. *Macromolecules* **1988**, *21*, 2610–2619. [CrossRef]
11. Galuschko, A.; Spirin, L.; Kreer, T.; Johner, A.; Pastorino, C.; Wittmer, J.; Baschnagel, J. Frictional Forces between Strongly Compressed, Nonentangled Polymer Brushes: Molecular Dynamics Simulations and Scaling Theory. *Langmuir* **2010**, *26*, 6418–6429. [CrossRef] [PubMed]
12. Kreer, T. Polymer-Brush Lubrication: A Review of Recent Theoretical Advances. *Soft Matter* **2016**, *12*, 3479–3501. [CrossRef] [PubMed]
13. Mari, R.; Seto, R.; Morris, J.F.; Denn, M.M. Shear Thickening, Frictionless and Frictional Rheologies in Non-Brownian Suspensions. *J. Rheol.* **2014**, *58*, 1693–1724. [CrossRef]
14. Singh, A.; Mari, R.; Denn, M.M.; Morris, J.F. A Constitutive Model for Simple Shear of Dense Frictional Suspensions. *J. Rheol.* **2018**, *62*, 457–468. [CrossRef]
15. Radhakrishnan, R.; Royer, J.R.; Poon, W.C.K.; Sun, J. Force Chains and Networks: Wet Suspensions through Dry Granular Eyes. *Granul. Matter* **2020**, *22*, 29. [CrossRef]
16. Freundlich, H.; Röder, H.L. Dilatancy and Its Relation to Thixotropy. *Trans. Faraday Soc.* **1938**, *34*, 308–316. [CrossRef]
17. Fall, A.; Huang, N.; Bertrand, F.; Ovarlez, G.; Bonn, D. Shear Thickening of Cornstarch Suspensions as a Reentrant Jamming Transition. *Phys. Rev. Lett.* **2008**, *100*, 018301. [CrossRef] [PubMed]
18. Egres, R.G.; Wagner, N.J. The Rheology and Microstructure of Acicular Precipitated Calcium Carbonate Colloidal Suspensions through the Shear Thickening Transition. *J. Rheol.* **2005**, *49*, 719–746. [CrossRef]

19. Bossis, G.; Boustingorry, P.; Grasselli, Y.; Meunier, A.; Morini, R.; Zubarev, A.; Volkova, O. Discontinuous Shear Thickening in the Presence of Polymers Adsorbed on the Surface of Calcium Carbonate Particles. *Rheol. Acta* **2017**, *56*, 415–430. [CrossRef]
20. Neuville, M.; Bossis, G.; Persello, J.; Volkova, O.; Boustingorry, P.; Mosquet, M. Rheology of a Gypsum Suspension in the Presence of Different Superplasticizers. *J. Rheol.* **2012**, *56*, 435–451. [CrossRef]
21. Frith, W.J.; d'Haene, P.; Buscall, R.; Mewis, J. Shear Thickening in Model Suspensions of Sterically Stabilized Particles. *J. Rheol.* **1996**, *40*, 531–548. [CrossRef]
22. Wagstaff, I.; Chaffey, C.E. Shear Thinning and Thickening Rheology: I. Concentrated Acrylic Dispersions. *J. Colloid Interface Sci.* **1977**, *59*, 53–62. [CrossRef]
23. Bergström, L. Shear Thinning and Shear Thickening of Concentrated Ceramic Suspensions. *Colloids Surf. A Physicochem. Eng. Asp.* **1998**, *133*, 151–155. [CrossRef]
24. Boersma, W.H.; Baets, P.J.M.; Laven, J.; Stein, H.N. Time-dependent Behavior and Wall Slip in Concentrated Shear Thickening Dispersions. *J. Rheol.* **1991**, *35*, 1093–1120. [CrossRef]
25. Laun, H.M.; Bung, R.; Schmidt, F. Rheology of Extremely Shear Thickening Polymer Dispersionsa)(Passively Viscosity Switching Fluids). *J. Rheol.* **1991**, *35*, 999–1034. [CrossRef]
26. Fagan, M.E.; Zukoski, C.F. The Rheology of Charge Stabilized Silica Suspensions. *J. Rheol.* **1997**, *41*, 373–397. [CrossRef]
27. Lootens, D.; Van Damme, H.; Hébraud, P. Giant Stress Fluctuations at the Jamming Transition. *Phys. Rev. Lett.* **2003**, *90*, 178301. [CrossRef]
28. Bender, J.; Wagner, N.J. Reversible Shear Thickening in Monodisperse and Bidisperse Colloidal Dispersions. *J. Rheol.* **1996**, *40*, 899–916. [CrossRef]
29. Bossis, G.; Grasselli, Y.; Meunier, A.; Volkova, O. Outstanding Magnetorheological Effect Based on Discontinuous Shear Thickening in the Presence of a Superplastifier Molecule. *Appl. Phys. Lett.* **2016**, *109*, 111902. [CrossRef]
30. O'Brie, V.T.; Mackay, M.E. Stress Components and Shear Thickening of Concentrated Hard Sphere Suspensions. *Langmuir* **2000**, *16*, 7931–7938. [CrossRef]
31. Richards, J.A.; O'Neill, R.E.; Poon, W.C.K. Turning a Yield-Stress Calcite Suspension into a Shear-Thickening One by Tuning Inter-Particle Friction. *Rheol Acta* **2021**, *60*, 97–106. [CrossRef]
32. Desai, P.R.; Das, S. Lubrication in Polymer-Brush Bilayers in the Weak Interpenetration Regime: Molecular Dynamics Simulations and Scaling Theories. *Phys. Rev. E* **2018**, *98*, 022503. [CrossRef] [PubMed]
33. Morillas, J.R.; de Vicente, J. Magnetorheology: A Review. *Soft Matter* **2020**, *16*, 9614–9642. [CrossRef] [PubMed]
34. Kumar, J.S.; Paul, P.S.; Raghunathan, G.; Alex, D.G. A Review of Challenges and Solutions in the Preparation and Use of Magnetorheological Fluids. *Int. J. Mech. Mater. Eng.* **2019**, *14*, 13. [CrossRef]
35. Bossis, G.; Ciffreo, A.; Grasselli, Y.; Volkova, O. Analysis of the Rheology of Magnetic Bidisperse Suspensions in the Regime of Discontinuous Shear Thickening. *Rheol. Acta* **2023**, *62*, 205–223. [CrossRef]
36. Bossis, G.; Grasselli, Y.; Volkova, O. Discontinuous Shear Thickening (DST) Transition with Spherical Iron Particles Coated by Adsorbed Brush Polymer. *Phys. Fluids* **2022**, *34*, 113317. [CrossRef]
37. Wyart, M.; Cates, M.E. Discontinuous Shear Thickening without Inertia in Dense Non-Brownian Suspensions. *Phys. Rev. Lett.* **2014**, *112*, 098302. [CrossRef]
38. Masel, R.I. *Principles of Adsorption and Reaction on Solid Surfaces*; John Wiley & Sons: Hoboken, NJ, USA, 1996; Volume 3.
39. De Gennes, P.G. Polymers at an Interface; a Simplified View. *Adv. Colloid Interface Sci.* **1987**, *27*, 189–209. [CrossRef]
40. Patel, S.; Tirrell, M.; Hadziioannou, G. A Simple Model for Forces between Surfaces Bearing Grafted Polymers Applied to Data on Adsorbed Block Copolymers. *Colloids Surf.* **1988**, *31*, 157–179. [CrossRef]
41. Desai, P.R.; Sinha, S.; Das, S. Compression of Polymer Brushes in the Weak Interpenetration Regime: Scaling Theory and Molecular Dynamics Simulations. *Soft Matter* **2017**, *13*, 4159–4166. [CrossRef]
42. Flory, P.J. *Principles of Polymer Chemistry*; Cornell University Press: Ithaca, NY, USA, 1953.
43. Mark, J.E.; Flory, P.J. The Configuration of the Polyoxyethylene Chain. *J. Am. Chem. Soc.* **1965**, *87*, 1415–1423. [CrossRef]
44. Lee, H.; Venable, R.M.; MacKerell, A.D.; Pastor, R.W. Molecular Dynamics Studies of Polyethylene Oxide and Polyethylene Glycol: Hydrodynamic Radius and Shape Anisotropy. *Biophys. J.* **2008**, *95*, 1590–1599. [CrossRef] [PubMed]
45. White, L.R. On the Deryaguin Approximation for the Interaction of Macrobodies. *J. Colloid Interface Sci.* **1983**, *95*, 286–288. [CrossRef]
46. Binder, K.; Milchev, A. Polymer Brushes on Flat and Curved Surfaces: How Computer Simulations Can Help to Test Theories and to Interpret Experiments. *J. Polym. Sci. B Polym. Phys.* **2012**, *50*, 1515–1555. [CrossRef]
47. Pedersen, J.S.; Sommer, C. Temperature Dependence of the Virial Coefficients and the Chi Parameter in Semi-Dilute Solutions of PEG. In *Scattering Methods and the Properties of Polymer Materials*; Springer: Berlin/Heidelberg, Germany, 2005; pp. 70–78, ISBN 978-3-540-25323-5.
48. Hough, D.B.; White, L.R. The Calculation of Hamaker Constants from Liftshitz Theory with Applications to Wetting Phenomena. *Adv. Colloid Interface Sci.* **1980**, *14*, 3–41. [CrossRef]
49. Cowley, M.D. Ferrohydrodynamics. By RE ROSENSWEIG. Cambridge University Press, 1985. 344 Pp. £ 45. *J. Fluid Mech.* **1989**, *200*, 597–599. [CrossRef]

50. Devanand, K.; Selser, J.C. Asymptotic Behavior and Long-Range Interactions in Aqueous Solutions of Poly(Ethylene Oxide). *Macromolecules* **1991**, *24*, 5943–5947. [CrossRef]
51. Sherck, N.; Webber, T.; Brown, D.R.; Keller, T.; Barry, M.; DeStefano, A.; Jiao, S.; Segalman, R.A.; Fredrickson, G.H.; Shell, M.S.; et al. End-to-End Distance Probability Distributions of Dilute Poly(Ethylene Oxide) in Aqueous Solution. *J. Am. Chem. Soc.* **2020**, *142*, 19631–19641. [CrossRef]